# C-Terminal Alternative Splicing Changes the Gating Properties of a Human Spinal Cord Calcium Channel $\alpha$1A Subunit

**Howard S. Krovetz, Thomas D. Helton, Anne L. Crews, and William A. Horne**

*Department of Anatomy, Physiological Sciences, and Radiology, North Carolina State University College of Veterinary Medicine, Raleigh, North Carolina 27606*

The calcium channel $\alpha_{1A}$ subunit gene codes for proteins with diverse structure and function. This diversity may be important for fine tuning neurotransmitter release at central and peripheral synapses. The $\alpha_{1A}$ C terminus, which serves a critical role in processing information from intracellular signaling molecules, is capable of undergoing extensive alternative splicing. The purpose of this study was to determine the extent to which C-terminal alternative splicing affects some of the fundamental biophysical properties of $\alpha_{1A}$ subunits. Specifically, the biophysical properties of two alternatively spliced $\alpha_{1A}$ subunits were compared. One variant was identical to an isoform identified previously in human brain, and the other was a novel isoform isolated from human spinal cord. The variants differed by two amino acids (NP) in the extracellular linker between transmembrane segments IVS3 and IVS4 and in two C-terminal regions encoded by exons 37 and 44. Expression in *Xenopus* oocytes demonstrated that the two variants were similar with respect to current–voltage relationships and the voltage dependence of steady-state activation and inactivation. However, the rates of activation, inactivation, deactivation, and recovery from inactivation were all significantly slower for the spinal cord variant. A chimeric strategy demonstrated that the inclusion of the sequence encoded by exon 44 specifically affects the rate of inactivation. These findings demonstrate that C-terminal structural changes alone can influence the way in which $\alpha_{1A}$ subunits respond to a depolarizing stimulus and add to the developing picture of the C terminus as a critical domain in the regulation of $Ca^{2+}$ channel function.

*Key words: spinal cord; cerebellum; calcium channel; $\alpha$1A subunit; voltage clamp; alternative splicing; C terminus*

Multiple types of high-voltage-activated $Ca^{2+}$ channels (L, N, P, Q, and R) coordinate a variety of $Ca^{2+}$-dependent processes, including gene expression, signal propagation, and neurotransmitter release (Tsien et al., 1991; Zhang et al., 1993; Dunlap et al., 1995). These channels can be distinguished by their biophysical and pharmacological properties. L- and R-type channels, found on cell bodies and proximal dendrites, regulate gene transcription and signal propagation (Westenbroek et al., 1990; Murphy et al., 1991; Yokoyama et al., 1995), whereas synaptic N-, P-, and Q-type channels regulate neurotransmitter release (Turner et al., 1992; Takahashi and Momiyama, 1993; Wheeler et al., 1994). The $Ca^{2+}$ channel complex consists of four subunits, $\alpha_1$, $\alpha_2/\delta$, $\beta$, and $\gamma$. With the exception of P- and Q-type channels, the different neuronal $Ca^{2+}$ channel phenotypes arise primarily from the expression of five unique $\alpha_1$ subunit genes (Tsien et al., 1991; Jun et al., 1999). These genes (A–E) are differentially distributed throughout brain and spinal cord (Murphy et al., 1991; Takahashi and Momiyama, 1993; Westenbroek et al., 1998) and encode large proteins consisting of four homologous domains (I–IV) containing six transmembrane segments each (S1–S6) (Tsien et al., 1991; Zhang et al., 1993).

Alternative splicing of the $\alpha_{1A}$ gene results in the expression of multiple $Ca^{2+}$ channel phenotypes (Sutton et al., 1998; Bourinet et al., 1999; Hans et al., 1999; Jun et al., 1999). Splicing of two amino acids (NP) in the $\alpha_{1A}$ IVS3–IVS4 linker affects rates of activation and inactivation, the voltage dependence of inactivation, and the affinity of $\alpha_{1A}$ for $\omega$-Aga IVA (Sutton et al., 1998; Bourinet et al., 1999; Hans et al., 1999; Lin et al., 1999). The biophysical and pharmacological properties of $\alpha_{1A}$ $Ca^{2+}$ channels are also influenced by intracellular signaling molecules. Coexpression of $\alpha_{1A}$ with different $\beta$ subunit subtypes alters inactivation rates and $\omega$-Aga IVA affinity (Moreno et al., 1997). Generally, $\alpha_{1A}$ subunit function is inhibited by interactions with G-proteins or syntaxin-1A (Zhang et al., 1996; Qin et al., 1997; Sutton et al., 1999) and enhanced by protein kinase C (Zamponi et al., 1997; Bourinet et al., 1999). Calcium-activated calmodulin has dual effects on $\alpha_{1A}$ subunit function (Lee et al., 1999).

Determination of genomic exon–intron boundaries (Ophoff et al., 1996) and isolation of several $\alpha_{1A}$ C-terminal splice variants (Zhuchenko et al., 1997) suggest that there are four exons between IVS3–IVS4 and the C-terminal stop codon that undergo alternative splicing. This implies that 16 combinations of these four exons are possible. Eight combinations have been isolated previously from human brain (Ophoff et al., 1996; Zhuchenko et al., 1997; Hans et al., 1999). In this study, a ninth is isolated from human spinal cord. Biophysical characterization of this $\alpha_{1A}$ variant reveals that its rates of activation, inactivation, deactivation, and recovery from inactivation are all significantly slower than that of an $\alpha_{1A}$ variant from cerebellum. The rate of inactivation was especially affected by sequence encoded by a single exon. These findings suggest that variation in $\alpha_{1A}$ C-terminal structure provides an added mechanism for functional diversity among neuronal $Ca^{2+}$ channel subtypes.

## MATERIALS AND METHODS

*Human spinal cord library screening.* Calcium channel subunit cDNAs were isolated from an oligo-dT and random-primed human spinal cord λgt11 5′ stretch cDNA library (Clontech, Palo Alto, CA) by the use of a nonradioactive digoxigenin-labeling and colorimetric detection system (Roche Molecular Biochemicals, Indianapolis, IN). The library was constructed from mRNA isolated from whole spinal cords pooled from 26 male or female Caucasians, ages 16–75, who died of sudden death syndrome. The insert size range of the library was 0.8–7.0 kb (average size of 1.7 kb). Plaque-purified phage DNAs were isolated using a Lambda Prep Kit (Qiagen, Santa Clara, CA) and digested with the restriction endonuclease *Eco*RI (Roche Molecular Biochemicals, supplier of all endonucleases used). Southern blot analysis was used to assess insert size. cDNA isolates were ligated into pBluescriptII (Stratagene, La Jolla, CA) for sequencing. The

Received Jan. 13, 2000; revised Aug. 1, 2000; accepted Aug. 4, 2000.

This work was supported by National Institutes of Health Grant R29-NS 32094, North Carolina State University Faculty Research and Professional Development Grant 09223-350791, and North Carolina Biotechnology Center Academic Research Initiation Grant 9905 ARG 0044. We would like to thank Drs. Robert Rosenberg and Mark Chapman for advice in the preparation of this manuscript.

Correspondence should be addressed to Dr. William A. Horne, College of Veterinary Medicine, North Carolina State University, 4700 Hillsborough Street, Raleigh, NC 27606. E-mail: Bill_Horne@ncsu.edu.

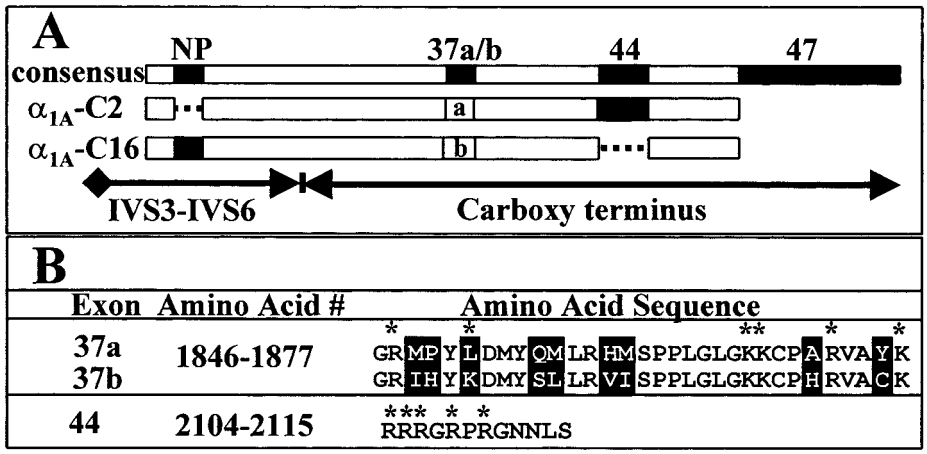


*Figure 1.* Alternative splicing of $\alpha_{1A}$ domain IV and C-terminal exons. *A*, Alternatively spliced exon patterns of $\alpha_{1A\text{-}C2}$ (*middle bar*) and $\alpha_{1A\text{-}C16}$ (*bottom bar*) cDNAs relative to a consensus protein that is a composite of known exons (*top bar*). This figure is drawn on the basis of our data and that of others (Ophoff et al., 1996; Zhuchenko et al., 1997; Hans et al., 1999). Note that the NP sequence is located in the extracellular loop between transmembrane domains IVS3 and IVS4. *B*, The amino acid sequences of exons 37a, 37b, and 44. Regions of variation are highlighted in *black*. Charged amino acids are denoted by an *asterisk*.

inserts were subjected to exonuclease III/SI nuclease digestion (Erase-A-Base; Promega, Madison, WI) before sequencing. PCR-based cycle sequencing (FS chemistry; PE Biosystems, Foster City, CA) with universal primers and custom internal primers (Genosys, The Woodlands, TX) was used for each clone. Sequence was obtained using an ABI Prism 310 Genetic DNA analyzer, and data were analyzed using ABI Prism DNA Sequencing Software (version 2.12; PE Biosystems). Sequence comparisons, alignments, and restriction maps were performed using Lasergene Software (DNAStar, Madison, WI). 5′ RACE (Roche Molecular Biochemicals) was used with human spinal cord poly($A^+$) RNA (Clontech) to create a 5′ probe for the $\alpha_{1A}$ screening. This RNA came from a pool of 92 male or female Caucasians, ages 16–75, who died from sudden death syndrome.

The library-screening process was initiated with a cDNA probe ($\alpha_1$-EST) obtained from the NCBI dbEST database (1.8 kb human fetal brain $\alpha_{1A}$ fragment; GenBank number H14053). Clone $\alpha_1$-9, extending from nucleotide 3416 to the 3′-untranslated region, was the longest of 24 3′ cDNAs isolated in the first rounds of screening. Five $\alpha_1$ cDNAs were isolated in a second round, in which a 1 kb 5′ *Eco*RI fragment of clone $\alpha_1$-9 was used as the probe. The longest clone isolated in this round, extending from nucleotides 2399 to 4551, was subsequently labeled and used as a probe to identify $\alpha_1$-38 (which contained an *Eco*RI/*Eco*RI fragment from 1800 to 4551). To isolate the 5′ portion of the $\alpha_{1A}$ sequence, a probe containing nucleotides 946 to 1800 was created by reverse transcription-PCR with human spinal cord RNA. Library screening with this probe yielded 14 cDNAs, one of which, clone $\alpha_1$-80, extended from the 5′-untranslated region to a region beyond the *Eco*RI site at nucleotide 1800.

*Clone construction and sequencing.* Full-length spinal cord $\alpha_{1A}$ cDNAs were assembled in several steps. Initially, PCR was performed using PFU Polymerase (Stratagene) and custom primers (Genosys) to truncate the 5′-untranslated region of $\alpha_1$-80 and to insert an idealized Kozak (Kozak, 1991) sequence into the shortened 5′ end of the construct. The resulting 1.1 kb fragment was then ligated into the pT-Adv vector (Clontech) and sequenced to ensure that there were no polymerase errors. This PCR product was cut with the restriction endonuclease *Not*I, and the resulting fragment was ligated into *Eco*RV/*Not*I-prepared pBluescriptII. The untruncated $\alpha_1$-80 was cut with *Not*I, and the resulting 900 bp fragment was then ligated into the shortened 5′ clone by the use of *Not*I. The resulting clone (referred to as 5′short) spans from the shortened 5′-untranslated sequence to the *Eco*RI site at nucleotide1800.

In the next step, a 3′ cDNA extending from nucleotide 3826 to the 3′-untranslated region of the clone, $\alpha_1$-10, was cut with *Not*I to eliminate the *Eco*RI site located in the polylinker of pBluescriptII. The construct was then cut with *Sac*I, blunted using the Klenow fragment (Roche Molecular Biochemicals), and cut with *Eco*RI to yield a 3.5 kb fragment spanning from the *Eco*RI site at 4551 to the 3′-untranslated region. This fragment was ligated into *Eco*RI/*Sma*I-prepared pBluescriptII, removed with *Eco*RI/*Bam*HI, and ligated into the *Eco*RI/*Bam*HI-cut vector containing 5′short. Thus, the resulting construct (5′short + 3′) extended from the shortened 5′-untranslated region to the *Eco*RI site at 1800 and continued from the *Eco*RI site at 4551 to the 3′-untranslated region. In the final step, an *Eco*RI fragment of $\alpha_1$-38 extending from 1801 to 4550 was cloned into *Eco*RI-cut 5′short + 3′. The fully constructed clone $\alpha_{1A\text{-}C1}$ was then sequenced to ensure the fidelity of the construction process. Exchanging the C-terminal domain of $\alpha_{1A\text{-}C1}$ with that of $\alpha_1$-EST and $\alpha_1$-9 created $\alpha_{1A\text{-}C2}$ and $\alpha_{1A\text{-}C16}$, respectively. Thus, both $\alpha_{1A\text{-}C2}$ and $\alpha_{1A\text{-}C16}$ are constructed of the same cDNAs up to nucleotide 4550 but then contain segments of different cDNAs beyond this point.

The rabbit $Ch\beta_{1a}$ and $\alpha_{2a}/\delta$ clones used in this study were provided by T. Tanabe (Tokyo Medical and Dental University, Tokyo, Japan). The $Ch\beta_{1b}$, $Ch\beta_3$, and $Ch\beta_4$ subunits were cloned from the same human spinal cord library described above and are nearly identical to previously reported sequences ($Ch\beta_{1b}$, GenBank number M923303; $Ch\beta_3$, GenBank number U07139; and $Ch\beta_4$, GenBank number U95020).

*Electrophysiology and data analysis.* Standard *Xenopus laevis* oocyte expression methods were used to characterize the $\alpha_{1A}$ splice variants. Briefly, full-length $\alpha_{1A}$ subunit cDNA was *in vitro* transcribed (Ambion, Austin, TX). The resulting cRNA was injected into defolliculated *X. laevis* oocytes (stage V–VI) along with equimolar ratios of rabbit $\alpha_{2a}/\delta$ and $Ch\beta$ cRNAs (0.40 μg/ml $\alpha_{1A}$; 0.16 μg/ml $\alpha_{2a}/\delta$; 0.08 μg/ml $Ch\beta$ in a total of 46 nl). $Ca^{2+}$ channel currents were recorded by standard two-microelectrode voltage-clamp techniques using a Warner amplifier (OC-725B) at room temperature (20–22°C), and data were collected using pCLAMP6 software (Axon Instruments, Foster City, CA). The bath solution contained the following: 40 mM $Ba(OH)_2$, 40 mM TEA-OH, 2 mM KOH, and 5 mM HEPES, with pH adjusted to 7.4 with methanesulphonic acid. Microelectrodes were filled with 3 M KCl, and the resistances of the current and voltage electrodes were 0.3–1.5 MΩ. Data were filtered at 2 kHz and sampled at 10 kHz. Currents were recorded 6–18 d after injection. The holding potential of all experiments was −100 mV unless otherwise noted. Control oocytes ($\alpha_{1A}$ alone or uninjected oocytes) did not yield currents >50 nA. Because of lower expression levels when $Ch\beta$ subunits other than the rabbit $Ch\beta_{1a}$ were used, currents as low as 150 nA were included in the initial portion of the study. Only currents >0.5 μA were analyzed for the remainder of this work. To diminish the contamination caused by the $Ca^{2+}$-activated $Cl^-$ channels, currents that exhibited slow deactivation ($\tau > 10$ msec) were excluded from analysis. The leak current and capacitive current transients were subtracted on-line by a standard P/4 protocol. Data were analyzed using pCLAMP6 and Excel 7.0 (Microsoft, Redmond, WA). For statistical analysis, a one-way ANOVA test was used followed by a Fisher's PLSD test using Statview software (SAS Institute, Cary, NC).

## RESULTS

Two $\alpha_{1A}$ C-terminal splice variants, $\alpha_{1A\text{-}C2}$ and $\alpha_{1A\text{-}C16}$, are the focus of this study (Fig. 1*A*). These variants were assembled from a parent spinal cord construct, $\alpha_{1A\text{-}C1}$, and thus are identical up to homology domain IV. Sequencing of the $\alpha_{1A\text{-}C1}$ cDNA through domain IV revealed only three differences when compared with an $\alpha_{1A}$ cDNA isolated from human cerebellum (GenBank number AF004883). A deletion (ΔG419) identified previously in rat brain was found in the region encoding the intracellular linker between homology domains I and II (Bourinet et al., 1999). A mutation resulting in a charge change (M537R) was found in the region encoding transmembrane segment IIS2. A nine nucleotide deletion resulting in the loss of amino acids 726–728 (VEA) was found in the region encoding the intracellular linker between homology domains II and III. This deletion has been identified in another $\alpha_{1A}$ variant from human brain (GenBank number U79666). The spinal cord $\alpha_{1A\text{-}C1}$ cDNA did not contain a six nucleotide insertion that codes for the amino acid sequence NP in the extracellular linker between IVS3 and IVS4.

The $\alpha_1$-EST and $\alpha_1$-9 C-terminal cDNAs used to construct $\alpha_{1A\text{-}C2}$ and $\alpha_{1A\text{-}C16}$, respectively, differed from the C terminus of $\alpha_{1A\text{-}C1}$ and other $\alpha_{1A}$ clones in sequences that could be traced to specific exon–intron boundaries (Ophoff et al., 1996). The $\alpha_1$-EST cDNA did not extend to domain IV, and therefore $\alpha_{1A\text{-}C2}$, like $\alpha_{1A\text{-}C1}$, lacks NP (Fig. 1*A*). The $\alpha_1$-9 cDNA contained the NP exon, and this region is therefore present in $\alpha_{1A\text{-}C16}$. The $\alpha_1$-EST cDNA contained one version of exon 37 (37a), whereas $\alpha_1$-9 contained a second (37b). There are nine amino acid changes in this

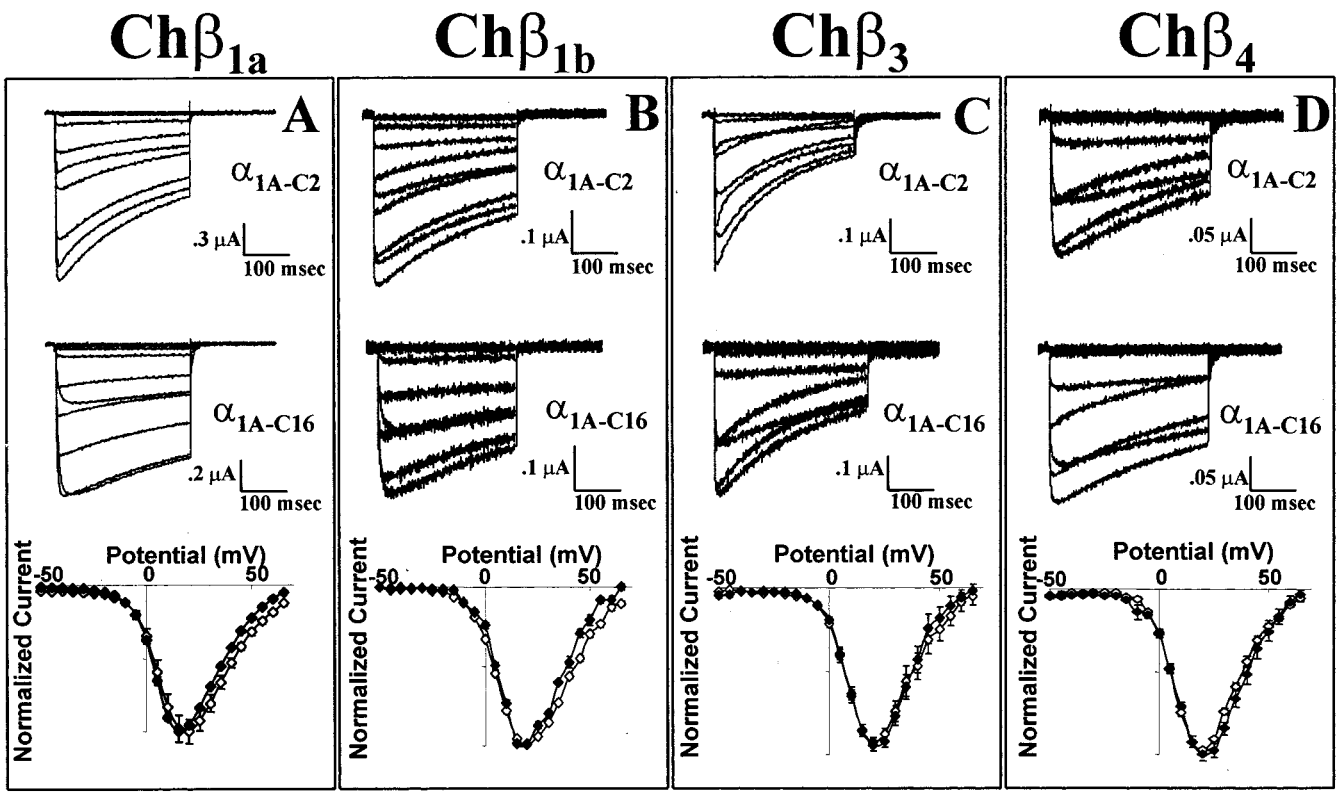


*Figure 2.* Biophysical properties of the $\alpha_{1A\text{-}C2}$ and $\alpha_{1A\text{-}C16}$ subunits coexpressed with rabbit $\alpha_{2a}/\delta$ and Ch$\beta_{1a}$, Ch$\beta_{1b}$, Ch$\beta_3$, or Ch$\beta_4$ subunits. *A–D*, Representative current *traces* of $\alpha_{1A\text{-}C2}$ (*top*) and $\alpha_{1A\text{-}C16}$ (*middle*) between −40 and +40 mV with the Ch$\beta_{1a}$ (*A*), Ch$\beta_{1b}$ (*B*), Ch$\beta_3$ (*C*), or Ch$\beta_4$ (*D*) subunit. Normalized current–voltage relationships (*bottom*) of $\alpha_{1A\text{-}C2}$ (*open diamonds*) and $\alpha_{1A\text{-}C16}$ (*filled diamonds*) with the Ch$\beta_{1a}$ ($n$ = 14 and 20, respectively), Ch$\beta_{1b}$ ($n$ = 21 and 14, respectively), Ch$\beta_3$ ($n$ = 10 and 10, respectively), or Ch$\beta_4$ ($n$ = 26 and 22, respectively) subunit.

region including one charge change (Fig. 1*B*, L1851K). The $\alpha_1$-EST cDNA contained 12 amino acids encoded by exon 44, whereas $\alpha_1$-9 did not. Interestingly, five of these amino acids are positively charged (Fig. 1*B*). A 3′ GGCAG insert in exon 46 that would extend the open reading frame to exon 47, although present in $\alpha_{1A\text{-}C1}$ (data not shown), was not found in either $\alpha_1$-EST or $\alpha_1$-9 (Fig. 1*A*). Thus, neither $\alpha_{1A\text{-}C2}$ nor $\alpha_{1A\text{-}C16}$ contains the ~240 amino acid domain encoded by exon 47. The end result is that $\alpha_{1A\text{-}C2}$ is identical to the human cerebellar clone described above, and $\alpha_{1A\text{-}C16}$ represents a novel spinal cord clone containing a unique arrangement of NP and C-terminal exons.

To determine the functional consequences of C-terminal splicing, both $\alpha_{1A\text{-}C2}$ and $\alpha_{1A\text{-}C16}$ were coexpressed with rabbit $\alpha_{2a}/\delta$ and a rabbit Ch$\beta_{1a}$ or a human Ch$\beta_{1b}$, Ch$\beta_3$, or Ch$\beta_4$ subunit in *Xenopus* oocytes. Representative current traces demonstrate that $\alpha_{1A\text{-}C2}$ inactivates more rapidly than does $\alpha_{1A\text{-}C16}$ when associated with Ch$\beta_{1a}$, Ch$\beta_{1b}$, or Ch$\beta_3$ subunits (Fig. 2*A–C*; see below). When coexpressed with the Ch$\beta_4$ subunit, the $\alpha_{1A\text{-}C2}$ complex appears to inactivate at approximately the same rate as $\alpha_{1A\text{-}C16}$ (Fig. 2*D*) although the low expression levels of this complex make interpretation difficult. As seen in Figure 2*A*, the deactivation rate of the $\alpha_{1A\text{-}C2}$ variant was slightly faster than that of $\alpha_{1A\text{-}C16}$ [$\tau_{\text{deactivation}}$ ($\alpha_{1A\text{-}C2}$) = 5.6 ± 0.3 msec at −80 mV ($n$ = 7); $\tau_{\text{deactivation}}$ ($\alpha_{1A\text{-}C16}$) = 6.6 ± 0.3 msec at −80 mV ($n$ = 6)]. When expressed with each of the Ch$\beta$ subunits, the current–voltage relationships of $\alpha_{1A\text{-}C2}$ and $\alpha_{1A\text{-}C16}$ were essentially indistinguishable (Fig. 2). With all Ch$\beta$ subunits, both $\alpha_{1A}$ variants had peak inward currents at +15 to +20 mV. Additionally, the voltages at which 1% of the maximal current was obtained were nearly identical (Ch$\beta_{1a}/\alpha_{1A\text{-}C2}$ = −19.2 ± 4.4 mV, whereas Ch$\beta_{1a}/\alpha_{1A\text{-}C16}$ = −19.5 ± 5.0 mV; this measurement was not obtained with the other Ch$\beta$ subunits because of poor expression levels). Coexpression of the rabbit Ch$\beta_{1a}$ subunit yielded currents two to five times higher than that with any of the human Ch$\beta$ subunits (Fig. 2). The goal of this study was to determine the effect of C-terminal $\alpha_{1A}$ splicing on the function of the channel, independent of Ch$\beta$ binding to the region. Therefore, the remainder of the study was performed with the Ch$\beta_{1a}$ subunit because it does not appear to bind to this region of the $\alpha_{1A}$ subunit and has the most robust expression levels (Walker et al., 1998).

The voltage dependency of activation, as determined from tail current measurements, was similar between $\alpha_{1A\text{-}C2}$ and $\alpha_{1A\text{-}C16}$ [Fig. 3*A*, $V_{1/2}$ ($\alpha_{1A\text{-}C2}$) = 9.5 ± 1.4 mV; $V_{1/2}$ ($\alpha_{1A\text{-}C16}$) = 7.3 ± 1.1 mV], as was the voltage dependency of steady-state inactivation (Fig. 3*B*, $V_{1/2}$ ($\alpha_{1A\text{-}C2}$) = −37.9 ± 1.4 mV; $V_{1/2}$ ($\alpha_{1A\text{-}C16}$) = −34.3 ± 1.5 mV]. The time constants of activation and inactivation were described with a single exponential (Fig. 3*C,D*). The time constants of activation of the $\alpha_{1A\text{-}C16}$ variant, however, were much slower than that of $\alpha_{1A\text{-}C2}$ and varied with membrane potential (Fig. 3*E*). The $\tau$ values of activation of $\alpha_{1A\text{-}C16}$ ranged from 6.15 ± 0.40 msec at 0 mV to 1.24 ± 0.06 msec at +30 mV, whereas those of $\alpha_{1A\text{-}C2}$ ranged from 2.07 ± 0.51 msec at 0 mV to 0.75 ± 0.12 msec at +30 mV. The time constants of inactivation of the $\alpha_{1A\text{-}C16}$ variant were also slower than that of $\alpha_{1A\text{-}C2}$ (Fig. 3*F*). The $\tau$ values of inactivation of $\alpha_{1A\text{-}C2}$ ranged from 347 ± 69 msec at −10 mV to 175 ± 11 msec at +50 mV, whereas those of $\alpha_{1A\text{-}C16}$ ranged from 984 ± 325 msec at −10 mV to 338 ± 46 msec at +50 mV. Analysis of the correlation between peak current and the $\tau$ of inactivation demonstrates that slow activation of the $Cl_{Ca}$ current did not contaminate the apparent rates of inactivation ($r$ = 0.304).

Because $\alpha_{1A}$ subunits are expressed primarily at synapses and high-frequency trains of action potentials govern neurotransmitter release, recovery from inactivation was characterized as a means of predicting how $\alpha_{1A\text{-}C2}$ versus $\alpha_{1A\text{-}C16}$ might respond to repetitive stimulation. Interestingly, at −40 and −60 mV, the rates of recovery from inactivation of $\alpha_{1A\text{-}C2}$ and $\alpha_{1A\text{-}C16}$ are not significantly different (Fig. 4*A,D*). However, at more negative potentials, the $\alpha_{1A\text{-}C2}$ subunit recovers from inactivation more rapidly than does the $\alpha_{1A\text{-}C16}$ subunit (Fig. 4*B–D*). A comparison of the fits of these

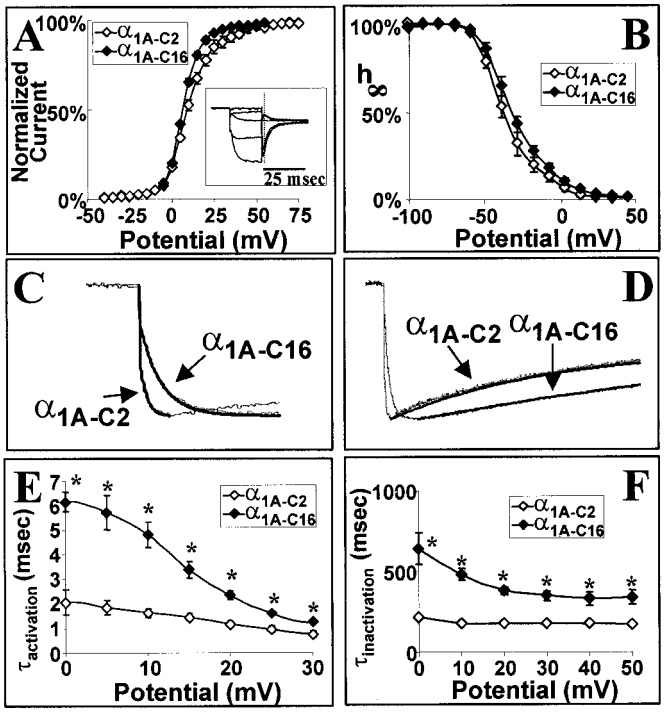


*Figure 3.* Voltage dependencies and rates of inactivation and activation of $\alpha_{1A-C2}$ and $\alpha_{1A-C16}$ subunit complexes. *A*, Voltage dependence of activation of $\alpha_{1A-C2}$ and $\alpha_{1A-C16}$ as measured from tail current measurements. *Inset*, Tail currents that were measured after the capacitive current (*dashed vertical line*) at 0 mV after a 20 msec depolarization to the test potential (−40 to +75 mV in 5 mV increments). Tail currents were normalized to the largest tail current in each series of test pulses. These data were fit with a Boltzmann equation: $\% I = 1/[1 + \exp(-(V_{test} - V_{1/2})/k)]$. *B*, Isochronal inactivation of $\alpha_{1A-C2}$ and $\alpha_{1A-C16}$. A 20 sec conditioning pulse ranged from −100 to +40 mV in 10 mV increments. The conditioning pulse was followed by a test pulse to +20 mV for 300 msec. Data were fit with a Boltzmann equation: $\% I = 1/[1 + \exp((V_{test} - V_{1/2})/k)]$. *C*, Single-exponential fits of activation of $\alpha_{1A-C2}$ and $\alpha_{1A-C16}$ at +20 mV. Fits are shown as *solid black lines*. *D*, Single-exponential fits of inactivation of $\alpha_{1A-C2}$ and $\alpha_{1A-C16}$ at +20 mV. Fits are shown as *solid black lines*. *E*, Average $\tau_{activation}$ of $\alpha_{1A-C2}$ and $\alpha_{1A-C16}$ between the voltages 0 and +30 mV. *Traces* were fit with a single exponential from the onset of the inward current to the time of peak current. For this and all following figures, the *asterisks* denote statistical significance ($p < 0.01$) by the use of an ANOVA test. *F*, Average $\tau_{inactivation}$ between −10 and +50 mV for $\alpha_{1A-C2}$ and $\alpha_{1A-C16}$. Each *point* represents a minimum of six recordings. The SEM for each *point* is shown unless the values were smaller than the *symbol*. *Traces* were fit with a single exponential from the peak inward current to the end of the depolarization.

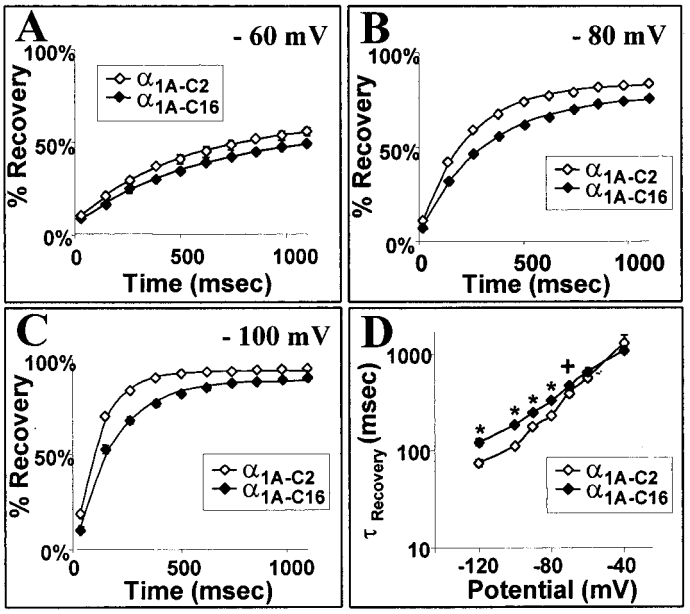


*Figure 4.* Voltage dependency of recovery from inactivation of the $\alpha_{1A-C2}$ and $\alpha_{1A-C16}$ subunit complexes. *A–C*, Average recoveries of $\alpha_{1A-C2}$ and $\alpha_{1A-C16}$ at −60 mV (*A*), −80 mV (*B*), and −100 mV (*C*). A two-pulse protocol was used with an initial test pulse of 600 msec to +30 mV followed by a conditioning pulse (ranging from −40 to −120 mV) of intervals ranging from 20 to 1100 msec. This was followed by a second 200 msec test pulse to +30 mV, $I_2$. The percentage recovery was measured as % Recovery = $(I_2 - I_{end\ of\ pulse\ I1})/(I_1 - I_{end\ of\ pulse\ I1})$. Each *point* shown is the average of six to nine different recordings. The SEM for each *point* is shown unless the values were smaller than the *symbol*. The *solid lines* are the single-exponential fits of the % Recovery. *D*, Voltage dependency of the rate of recovery from inactivation of $\alpha_{1A-C2}$ and $\alpha_{1A-C16}$. $\tau_{recovery}$ is the average value derived from single-exponential fits of individual experiments. The *asterisks* ($p < 0.01$) and *cross* ($p < 0.05$) denote statistical significance by the use of an ANOVA test.

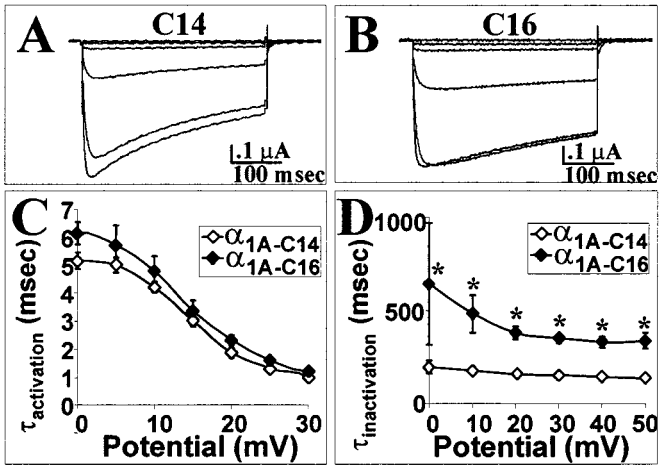


*Figure 5.* Exon 44 enhances the rate of inactivation. *A*, Current *traces* of $\alpha_{1A-C14}$, a clone that contains the 12 amino acids encoded by exon 44, between −50 and +40 mV. *B*, Current *traces* of $\alpha_{1A-C16}$, a clone that does not contain exon 44, between −50 and +40 mV. *C*, Average $\tau_{activation}$ of $\alpha_{1A-C14}$ and $\alpha_{1A-C16}$ between 0 and +30 mV. *D*, Average $\tau_{inactivation}$ between 0 and +50 mV for $\alpha_{1A-C14}$ and $\alpha_{1A-C16}$. Each *point* represents a minimum of five recordings. The SEM for each *point* is shown unless the values were smaller than the *symbol*. *Traces* were fit with a single exponential from the peak inward current to the end of the depolarization.

recovery rates with a single-exponential function reveals that the differences in recovery rates become more apparent at increasingly negative potentials (Fig. 4*D*), showing that the rate of recovery from inactivation of the $\alpha_{1A-C2}$ subunit is more voltage dependent than that of $\alpha_{1A-C16}$. Although this difference is greater at potentials not likely to be seen physiologically (−100 to −120 mV), the recovery rate is still significantly different between −70 and −90 mV: at −70 mV, $\tau_{recovery}$ $\alpha_{1A-C2}$ = 398 ± 19 msec, and $\tau_{recovery}$ $\alpha_{1A-C16}$ = 469 ± 23 msec; at −80 mV, $\tau_{recovery}$ $\alpha_{1A-C2}$ = 234 ± 11 msec, and $\tau_{recovery}$ $\alpha_{1A-C16}$ = 321 ± 19 msec; and at −90 mV, $\tau_{recovery}$ $\alpha_{1A-C2}$ = 178 ± 6 msec, and $\tau_{recovery}$ $\alpha_{1A-C16}$ = 251 ± 15 msec. The voltage dependence of the recovery from inactivation is shifted by ~10 mV in the physiological range (Fig. 4*D*).

Because the most obvious structural difference between $\alpha_{1A-C2}$ and $\alpha_{1A-C16}$ is the presence of the highly charged 12 amino acid segment encoded by exon 44 (Fig. 1*A*), a chimera was constructed to characterize the influence of this segment on channel gating. The chimera $\alpha_{1A-C14}$ is identical to $\alpha_{1A-C16}$ except that it contains the 12 amino acids encoded by exon 44. As expected, the voltage dependencies of activation and steady-state inactivation of $\alpha_{1A-C14}$ were similar to those of $\alpha_{1A-C16}$ [$V_{1/2activation}$ ($\alpha_{1A-C14}$) = 6.7 ± 1.3 mV; $V_{1/2inactivation}$ ($\alpha_{1A-C14}$) = −33.0 ± 1.1 mV]. The differences between the rates of activation (Fig. 5*C*) and deactivation [at −80 mV, $\tau_{deactivation}$ ($\alpha_{1A-C14}$) = 6.3 ± 0.4 msec] and the rates of recovery from inactivation (at −100 mV, $\tau_{recovery}$ = 216 ± 19 msec; at −80 mV, $\tau_{recovery}$ = 316 ± 31 msec; at −60 mV, $\tau_{recovery}$ = 520 ± 63 msec) were not statistically significant. The most striking differ-

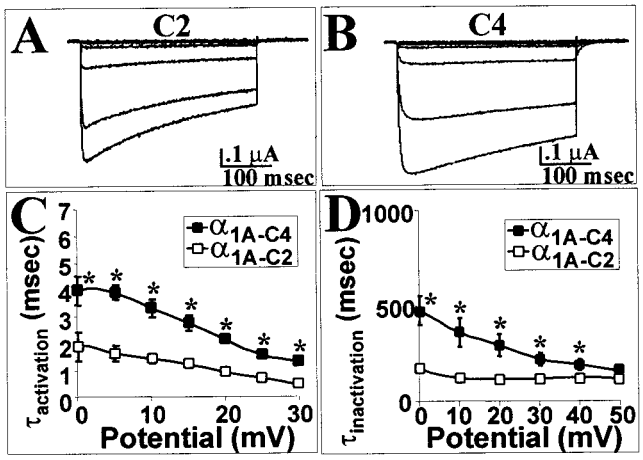


*Figure 6.* In a different C-terminal combination, the exon 44 slows the rate of activation but still enhances the rate of inactivation. *A*, Current *traces* of $\alpha_{1A\text{-}C2}$, a clone that contains the 12 amino acids encoded by exon 44, between −50 and +40 mV. *B*, Current *traces* of $\alpha_{1A\text{-}C4}$, a clone that does not contain exon 44, between −50 and +40 mV. *C*, Average $\tau_{activation}$ of $\alpha_{1A\text{-}C2}$ and $\alpha_{1A\text{-}C4}$ between 0 and +30 mV. *D*, Average $\tau_{inactivation}$ between 0 and +50 mV for $\alpha_{1A\text{-}C2}$ and $\alpha_{1A\text{-}C4}$. Each *point* represents a minimum of five recordings. The SEM for each *point* is shown unless the values were smaller than the *symbol*. *Traces* were fit with a single exponential from the peak inward current to the end of the depolarization.

ence between the two variants was the enhancement of the rate of inactivation of $\alpha_{1A\text{-}C14}$ relative to that of $\alpha_{1A\text{-}C16}$ (Fig. 5*A,B,D*). Moreover, these rates were similar to those of $\alpha_{1A\text{-}C2}$, ranging from 198 ± 14 msec at 0 mV to 133 ± 16 msec at +50 mV.

To determine whether the effects of the amino acid segment encoded by exon 44 on the rate of inactivation were background dependent, this exon was removed from $\alpha_{1A\text{-}C2}$ to create $\alpha_{1A\text{-}C4}$. Thus, $\alpha_{1A\text{-}C4}$ is identical to $\alpha_{1A\text{-}C2}$ except that it lacks the 12 amino acids encoded by exon 44. The effect of the removal of exon 44 was indeed to slow the rate of inactivation (Fig. 6*A,B,D*) without significantly affecting the voltage dependency of activation [$V_{1/2}$ ($\alpha_{1A\text{-}C4}$) = 7.7 ± 1.0 mV] or inactivation [$V_{1/2}$ ($\alpha_{1A\text{-}C4}$) = −31.4 ± 1.2 mV]. Interestingly, this construct had a slower rate of activation (Fig. 6*A–C*).

## DISCUSSION

The gating properties of neuronal $Ca^{2+}$ channels are determined by multiple structural domains within the $\alpha_1$ subunit (Tsien et al., 1991; Catterall, 1995). Our results indicate that C-terminus alternative splicing can influence some of these properties. The C terminus of the $\alpha_{1A}$ subunit is encoded by 12 exons, numbered 36–47 (Ophoff et al., 1996), of which 4 exons, 37, 44, 46, and 47, undergo alternative splicing (Zhuchenko et al., 1997). Depending on the pattern of splicing, the C terminus may vary from 436 to 517 amino acids. Binding sites for several intracellular signaling molecules, which affect channel gating, have been identified within this sequence. An EF-hand $Ca^{2+}$-binding motif can be aligned to sequence encoded by exons 36 and 37 (de Leon et al., 1995). Calmodulin has been shown to bind to a region of the C terminus encoded by exon 40 (Peterson et al., 1999) and to a calmodulin-binding domain (CBD) identified in the region encoded by exon 42 (Lee et al., 1999). Calcium-dependent binding of calmodulin to the CBD motif speeds inactivation and recovery from inactivation and produces a long-lasting facilitation of $Ca^{2+}$ current (Lee et al., 1999). Calcium channel $\beta_4$ subunit binding to a region encoded by exons 43–47 has been shown to enhance the rate of inactivation (Walker et al., 1998). In addition, the C terminus appears to be essential for modulation by $G_{\beta\gamma}$-proteins (Zhang et al., 1996), particularly those regions encoded by exons 45 and 46 (Qin et al., 1997). G-proteins modulate the kinetics of channel activation and inactivation, the voltage dependence of activation, and recovery from inactivation (Bean, 1989; Patil et al., 1998; Zamponi and Snutch, 1998). Polyglutamine tract expansions in exon 47 (Zhuchenko et al., 1997) shift the voltage dependence of activation to more negative potentials, dramatically increase current density (Piedras-Rentería et al., 1999), and alter activation and inactivation kinetics (Resituito et al., 1999). These latter effects appear to be dependent on coexpression of the $\beta_4$ subunit.

This study focuses on two naturally occurring splice variants of the $\alpha_{1A}$ subunit gene that differ in nucleotide sequences corresponding to the NP exon of the IVS3–IVS4 extracellular linker and C-terminal exons 37 and 44. One variant, $\alpha_{1A\text{-}C2}$, has been identified previously in human cerebellum but has not been expressed and characterized (Zhuchenko et al., 1997) (GenBank number U79663). It lacks the NP exon but contains exons 37a and 44. The other variant, $\alpha_{1A\text{-}C16}$, which has not been identified previously, contains the NP exon and exon 37b but lacks exon 44. Neither $\alpha_{1A\text{-}C2}$ nor $\alpha_{1A\text{-}C16}$ contains exon 47, which is present in the well characterized $\alpha_{1A}$ subunits BI-1 and BI-2 isolated from rabbit brain (Mori et al., 1991; Sather et al., 1993). Because of the central role of the $\alpha_{1A}$ C terminus in defining channel-gating characteristics, we hypothesized that the difference in splicing pattern between the two variants would be reflected by changes in their biophysical properties.

Expression in *Xenopus* oocytes demonstrated that $\alpha_{1A\text{-}C2}$ and $\alpha_{1A\text{-}C16}$ are similar with respect to current–voltage relationships and the voltage dependency of activation and inactivation. This is different from previously reported results. The presence of the NP exon shifted the voltage dependence of activation and inactivation of a rat brain $\alpha_{1A}$ subunit (Bourinet et al., 1999). In a study conducted with a human $\alpha_{1A}$ subunit, the NP exon only shifted the voltage dependence of inactivation (Hans et al., 1999). Taken together, these data suggest that regions in addition to NP are important for determining the voltage dependence of activation and inactivation. However, other differences, such as the isoform of the Ch$\beta$ subunit coexpressed with the $\alpha_{1A}$ subunit, differing expression systems, and the lack of complete inactivation at the end of the conditioning pulse could shift the voltage dependence of inactivation (Hans et al., 1999).

Further characterization reveals differences in the respective rates of activation, inactivation, deactivation, and recovery from inactivation of channels containing the $\alpha_{1A\text{-}C2}$ or $\alpha_{1A\text{-}C16}$ subunits. Complexes containing the $\alpha_{1A\text{-}C16}$ subunit activate more slowly than do those that contain $\alpha_{1A\text{-}C2}$. This may be explained, in part, by the presence of the NP amino acids in the extracellular IVS3–IVS4 linker, which have been shown to decrease the rate of activation of $\alpha_{1A}$ and $\alpha_{1B}$ channel complexes by ~1.5-fold at +10 mV (Hans et al., 1999; Lin et al., 1999). The $\alpha_{1A\text{-}C2}$ complex has an apparent rate of activation that is similar to that of other $\alpha_{1A}$ subunits that lack NP (1.6 ± 0.2 vs 1.2 ± 0.5 msec) (Hans et al., 1999). The activation rate of $\alpha_{1A\text{-}C16}$ is considerably slower than that of other subunits that contain NP (4.8 ± 0.5 vs 2.2 ± 1.1 msec) (Hans et al., 1999), suggesting that other regions of the C terminus also affect activation. Our results indicate that the region encoded by exon 44 appears to be acting in a modular manner to enhance the rate of inactivation of $\alpha_{1A}$ complexes twofold to threefold. It is unclear whether this results from a direct conformational change or whether the presence or absence of this charged sequence affects modulation by intracellular signaling molecules. Further experiments are required to resolve this issue. Interestingly, the regions encoded by exons 43–47 have been shown to bind $\beta_4$ and $\beta_{2a}$ subunits but not $\beta_1$ or $\beta_3$ subunits (Walker et al., 1998). Our results with the $\beta_1$ subunit suggest that changes in inactivation imparted by exon 44 are independent of C-terminal $\beta$ subunit binding. The deactivation rate of the $\alpha_{1A\text{-}C16}$ complex is slightly slower than that of $\alpha_{1A\text{-}C2}$. Because the settling time of the oocyte clamp is ~2 msec, these rates are likely to be faster than we report. Regardless, the $\alpha_{1A\text{-}C16}$ complexes are consistently slower over a wide voltage range (−60 to −100 mV; data not shown). Thus, as is true for the $\alpha_{1C}$ subunit of L-type $Ca^{2+}$ channels (Soldatov et al., 1997, 1998), C-terminal alternative splicing does affect the biophysical properties of channel complexes composed of $\alpha_{1A}$ subunits.

The slower activation, inactivation, and deactivation of $\alpha_{1A\text{-}C16}$ splice variants relative to $\alpha_{1A\text{-}C2}$ could translate to differences in neurotransmitter release at subtype-specific synapses. Although differences in channel number and density, second messenger effects, and $Ca^{2+}$ buffering make it difficult to predict what the combined effects of C-terminal splicing on $Ca^{2+}$ entry will be (Park and Dunlap, 1998; Lin et al., 1999), our results do allow for some generalizations to be made. The slower rate of activation of channels containing the $\alpha_{1A\text{-}C16}$ subunit should lead to a decrease in the initial rate of calcium influx. However, the slower inactivation rate of the $\alpha_{1A\text{-}C16}$ subunit would enhance later calcium entry, providing the channel does not recover from inactivation by passing through the open state (Slesinger and Lansman, 1991). The slower deactivation rate of $\alpha_{1A\text{-}C16}$ channel complexes would increase $Ca^{2+}$ flux through these channels at a time when the driving force is relatively large. Therefore, it is likely that in response to a single action potential, the initial rate of $Ca^{2+}$ entry would be slower through complexes containing the $\alpha_{1A\text{-}C16}$ subunit, but these channels would allow for a greater total $Ca^{2+}$ influx.

The rate of recovery from inactivation at negative potentials plays an important role in determining $Ca^{2+}$ influx and neurotransmitter release in response to a train of action potentials. The voltage dependence of the rate of recovery of channel complexes containing the $\alpha_{1A\text{-}C16}$ subunit differs from those containing $\alpha_{1A\text{-}C2}$. At less negative potentials, the two splice variants behave similarly. After 500 msec at $-60$ mV, ~30% of channels composed of either variant are fully recovered. However, at more negative potentials, complexes containing the $\alpha_{1A\text{-}C16}$ subunit recover more slowly. After 500 msec at $-80$ mV, ~73% of $\alpha_{1A\text{-}C2}$ complexes are recovered, compared with ~62% of $\alpha_{1A\text{-}C16}$ complexes. Thus, $Ca^{2+}$ entry after a train of action potentials would be less in nerve terminals expressing the $\alpha_{1A\text{-}C16}$ subunit relative to those expressing the $\alpha_{1A\text{-}C2}$ subunit. These differences may be important from the standpoint of $Ca^{2+}$-mediated synaptic plasticity.

Our results add to a developing picture of neuronal calcium channels that suggests that $\alpha_1$ subunit genes express channels with a wide array of structures and functions. These channels may have evolved to meet the specific needs of highly specialized synapses. Our results, combined with those of several laboratories (Bourinet et al., 1999; Hans et al., 1999), point to the fact that it is no longer sufficient to refer to $\alpha_{1A}$ channels as simply P- and Q-type. Minor splicing events in critical domains of the $\alpha_{1A}$ subunit alter both pharmacological and physiological properties in ways in which we are only beginning to understand. Determination of where specific $\alpha_{1A}$ subunit splice variants are expressed, how they respond to trains of action potentials, and how they interact with various signaling molecules should greatly enhance our understanding of the physiology of the synapse.

## REFERENCES


Bean BP (1989) Neurotransmitter inhibition of neuronal calcium currents by changes in channel voltage dependence. Nature 340:153–156.

Bourinet E, Soong TW, Sutton K, Slaymaker S, Mathews E, Monteil A, Zamponi GW, Nargeot J, Snutch TP (1999) Splicing of alpha 1A subunit gene generates phenotypic variants of P- and Q-type calcium channels. Nat Neurosci 2:407–415.

Catterall WA (1995) Structure and function of voltage-gated ion channels. Annu Rev Biochem 64:493–531.

de Leon M, Wang Y, Jones L, Perez-Reyes E, Wei X, Soong TW, Snutch TP, Yue DT (1995) Essential $Ca^{2+}$-binding motif for $Ca^{2+}$-sensitive inactivation of L-type $Ca^{2+}$ channels. Science 270:1502–1506.

Dunlap K, Luebke JI, Turner TJ (1995) Exocytotic $Ca^{2+}$ channels in mammalian central neurons. Trends Neurosci 18:89–98.

Hans M, Urrutia A, Deal C, Brust PF, Stauderman K, Ellis SB, Harpold MM, Johnson EC, Williams ME (1999) Structural elements in domain IV that influence biophysical and pharmacological properties of human alpha1A-containing high-voltage-activated calcium channels. Biophys J 76:1384–1400.

Jun K, Piedras-Renteria ES, Smith SM, Wheeler DB, Lee SB, Lee TG, Chin H, Adams ME, Scheller RH, Tsien RW, Shin HS (1999) Ablation of P/Q-type $Ca^{2+}$ channel currents, altered synaptic transmission, and progressive ataxia in mice lacking the $alpha_{1A}$-subunit. Proc Natl Acad Sci USA 96:15245–15250.

Kozak M (1991) An analysis of vertebrate mRNA sequences: intimations of translational control. J Cell Biol 115:887–903.

Lee A, Wong ST, Gallagher D, Li B, Storm DR, Scheuer T, Catterall WA (1999) $Ca^{2+}$/calmodulin binds to and modulates P/Q-type calcium channels. Nature 399:155–159.

Lin Z, Lin Y, Schorge S, Pan JQ, Beierlein M, Lipscombe D (1999) Alternative splicing of a short cassette exon in $\alpha$1B generates functionally distinct N-type calcium channels in central and peripheral neurons. J Neurosci 19:5322–5331.

Moreno H, Rudy B, Llinas R (1997) Beta subunits influence the biophysical and pharmacological differences between the P- and Q-type calcium currents expressed in a mammalian cell line. Proc Natl Acad Sci 94: 14042–14047.

Mori Y, Friedrich T, Kim MS, Mikami A, Nakai J, Ruth P, Bosse E, Hoffmann F, Flockerzi V, Furuichi T, Mikoshiba K, Imoto K, Tanabe T, Numa S (1991) Primary structure and functional expression from complementary DNA of a brain calcium channel. Nature 350:398–402.

Murphy TH, Worley PF, Baraban JM (1991) L-type voltage-sensitive $Ca^{2+}$ channels mediate synaptic activation of immediate early genes. Neuron 7:625–635.

Ophoff RA, Terwindt GM, Vergouwe MN, van Eijk R, Oefner PJ, Hoffman SMG, Lamerdin JE, Mohrenweiser HW, Bulman DE, Ferrari M, Haan J, Lindhout D, van Ommen G-J, Hofker MH, Ferrari MD, Frants RR (1996) Familial hemiplegic migraine and episodic ataxia type-2 are caused by mutations in the $Ca^{2+}$ channel gene CACNL1A4. Cell 87:543–552.

Park D, Dunlap K (1998) Dynamic regulation of calcium influx by G-proteins, action potential waveform, and neuronal firing frequency. J Neurosci 18:6757–6766.

Patil PG, Brody DL, Yue DT (1998) Preferential closed-state inactivation of neuronal calcium channels. Neuron 20:1027–1038.

Peterson BZ, DeMaria CD, Adelman JP, Yue DT (1999) Calmodulin is the $Ca^{2+}$ sensor for $Ca^{2+}$-dependent inactivation of L-type calcium channels. Neuron 22:549–558.

Piedras-Rentería ES, Watase K, Zoghbi HY, Lee CC, Tsien RW (1999) Alteration of expressed alpha1A $Ca^{2+}$ channel currents arising from expanded trinucleotide repeats in spinocerebellar ataxia type 6. Soc Neurosci Abstr 25:431.

Qin N, Platano D, Olcese R, Stefani E, Birnbaumer L (1997) Direct interaction of Gbetagamma with a C-terminal Gbetagamma-binding domain of the $Ca^{2+}$ channel alpha1 subunit is responsible for channel inhibition by G protein-coupled receptors. Proc Natl Acad Sci USA 94:8866–8871.

Resituito S, Thompson R, Charnet P, Gomez C (1999) Multiple SCA6-associated, alpha1A splice forms may have altered activation/inactivation kinetics. Soc Neurosci Abstr 25:431.

Sather WA, Tanabe T, Zhang JF, Mori Y, Adams ME, Tsien RW (1993) Distinctive biophysical and pharmacological properties of class A(BI) calcium channel alpha 1 subunits. Neuron 11:291–303.

Slesinger PA, Lansman JB (1991) Reopening of $Ca^{2+}$ channels in mouse cerebellar neurons at resting membrane potentials during recovery from inactivation. Neuron 7:755–762.

Soldatov NM, Zühlke RD, Bouron A, Reuter H (1997) Molecular structures involved in L-type calcium channel inactivation. Role of the carboxyl-terminal region encoded by exons 40–42 in alpha 1C in the kinetics and $Ca^{2+}$ dependence of inactivation. J Biol Chem 272:3560–3566.

Soldatov NM, Oz M, O'Brien KA, Abernethy DR, Morad M (1998) Molecular determinants of L-type $Ca^{2+}$ channel inactivation. Segment exchange analysis of the carboxyl-terminal cytoplasmic motif encoded by exons 40–42 of the human alpha1C subunit gene. J Biol Chem 273:957–963.

Sutton KG, Zamponi GW, Bourinet E, Soong TW, Snutch TP (1998) Alternative splicing of the $\alpha$1a gene generates distinct P- or Q-type sensitivity to omega-Agatoxin IVA. Soc Neurosci Abstr 24:16.

Sutton KG, McRory JE, Guthrie H, Murphy TH, Snutch TP (1999) P/Q-type calcium channels mediate the activity-dependent feedback of syntaxin-1A. Nature 401:800–804.

Takahashi T, Momiyama A (1993) Different types of calcium channels mediate central synaptic transmission. Nature 366:156–158.

Tsien RW, Ellinor PT, Horne WA (1991) Molecular diversity of voltage-dependent $Ca^{2+}$ channels. Trends Pharmacol Sci 12:349–354.

Turner TJ, Adams ME, Dunlap K (1992) Calcium channels coupled to glutamate release identified by omega-Aga-IVA. Science 258:310–313.

Walker D, Bichet D, Campbell KP, De Waard M (1998) A beta 4 isoform-specific interaction site in the carboxyl-terminal region of the voltage-dependent $Ca^{2+}$ channel alpha1A subunit. J Biol Chem 273:2361–2367.

Westenbroek RE, Ahlijanian MK, Catterall WA (1990) Clustering of L-type $Ca^{2+}$ channels at the base of major dendrites in hippocampal pyramidal neurons. Nature 347:281–284.

Westenbroek RE, Hoskins L, Catterall WA (1998) Localization of $Ca^{2+}$ channel subtypes on rat spinal motor neurons, interneurons, and nerve terminals. J Neurosci 18:6319–6330.

Wheeler DB, Randall A, Tsien RW (1994) Roles of N-type and Q-type $Ca^{2+}$ channels in supporting hippocampal synaptic transmission. Science 264:107–111.

Yokoyama CT, Westenbroek RE, Hell JW, Soong TW, Snutch TP, Catterall WA (1995) Biochemical properties and subcellular distribution of the neuronal class E calcium channel alpha 1 subunit. J Neurosci 15: 6419–6432.

Zamponi GW, Snutch TP (1998) Modulation of voltage-dependent calcium channels by G proteins. Curr Opin Neurobiol 8:351–356.

Zamponi GW, Bourinet E, Nelson D, Nargeot J, Snutch TP (1997) Crosstalk between G proteins and protein kinase C mediated by the calcium channel $\alpha$1 subunit. Nature 385:442–446.

Zhang JF, Randall AD, Ellinor PT, Horne WA, Sather RA, Tanabe T, Schwarz TL, Tsien RW (1993) Distinctive pharmacology and kinetics of cloned neuronal $Ca^{2+}$ channels and their possible counterparts in mammalian CNS neurons. Neuropharmacology 32:1075–1088.

Zhang JF, Ellinor PT, Aldrich RW, Tsien RW (1996) Multiple structural elements in voltage-dependent $Ca^{2+}$ channels support their inhibition by G proteins. Neuron 17:991–1003.

Zhuchenko O, Bailey J, Bonnen P, Ashizawa T, Stockton DW, Amos C, Dobyns WB, Subramony SH, Zoghbi HY, Lee CC (1997) Autosomal dominant cerebellar ataxia (SCA6) associated with small polyglutamine expansions in the alpha1A-voltage-dependent calcium channel. Nat Genet 15:62–69.